Volume 1 | Number 1 | Jan 2013 | Pages 1–100

Metallomics

Integrated biometal science
www.rsc.org/metallomics

ROYAL SOCIETY OF CHEMISTRY

This is an *Accepted Manuscript*, which has been through the Royal Society of Chemistry peer review process and has been accepted for publication.

Accepted Manuscripts are published online shortly after acceptance, before technical editing, formatting and proof reading. Using this free service, authors can make their results available to the community, in citable form, before we publish the edited article. We will replace this *Accepted Manuscript* with the edited and formatted *Advance Article* as soon as it is available.

You can find more information about *Accepted Manuscripts* in the **Information for Authors**.

Please note that technical editing may introduce minor changes to the text and/or graphics, which may alter content. The journal's standard **Terms & Conditions** and the **Ethical guidelines** still apply. In no event shall the Royal Society of Chemistry be held responsible for any errors or omissions in this *Accepted Manuscript* or any consequences arising from the use of any information it contains.

Metallomics

ARTICLE

X-Ray Fluorescence imaging and other analyses identify selenium and GPX1 as important in female reproductive function

M. J. Ceko,[a] K. Hummitzsch,[b] N. Hatzirodos,[b] W. Bonner,[b] J. B. Aitken,[3] D. L. Russell,[2] M. Lane,[2,4] R. J. Rodgers,[2] and H. H. Harris.[c,*]

Studies of selenium (Se) status indicate that Se is necessary for fertility but how precisely is not known. We aimed to show that Se was important in bovine female reproductive function. The elemental distribution in the bovine ovary (n = 45 sections) was identified by X-ray fluorescence (XRF) imaging. Se was consistently localized to the granulosa cell layer of large (> 10 mm) healthy follicles. Inductively Coupled Plasma - Mass Spectrometry revealed tenfold higher Se in the bovine follicle wall compared to corpora lutea. Gene expression analysis of selenoprotein genes *GPX1*, *GPX3*, *VIMP* and *SELM* in bovine granulosa cells revealed that only *GPX1* was significantly up-regulated in large healthy follicles compared to the small healthy or atretic follicles ($P < 0.05$). Western immunoblotting identified GPX1 protein in bovine granulosa cells of large healthy follicles, but not of small healthy follicles. To assess if GPX1 was important in human follicles, cumulus cells from women undergoing IVF/ICSI with single embryo transfer were collected. Oocytes and embryos were cultured and transferred independently in 30 patients undergoing elective single embryo transfer. Gene expression of *GPX1* was significantly higher in human cumulus cells from cumulus-oocyte complexes yielding a pregnancy ($P < 0.05$). We present the first XRF imaging of mammalian ovaries showing that Se is consistently localized to the granulosa cells of large healthy follicles. We conclude that Se and selenoproteins are elevated in large healthy follicles and may play a critical role as an antioxidant during late follicular development.

Introduction

Selenium (Se) is a trace element and an essential component of selenoproteins, playing an important role in such biological functions as: antioxidant defense; formation of thyroid hormones; immune response; DNA synthesis; fertility; and, reproduction.[1,2] The selenoproteins incorporate Se co-translationally as a selenocysteine residue that acts as a very efficient redox catalyst,[3] protecting cells against reactive oxygen species (ROS).[4,5] ROS such as the superoxide radical anion (O_2^-) and hydrogen peroxide (H_2O_2), are produced as by-products of normal cellular metabolism and can react spontaneously with DNA, RNA, protein, and lipids.[6] Oxidative stress occurs when levels of ROS overwhelm the cell's antioxidant defences.[7] Well-characterized selenoproteins include the families of: glutathione peroxidases; thioredoxin reductases; and, iodothyronine deiodinases. The essential role of selenoproteins in peroxide degradation, maintenance of cellular redox status, transcription regulation, and thyroid hormone deiodination is evident, but several additional unknown biochemical pathways remain to be elucidated.[8]

Information regarding the importance of Se in female reproduction is sparse.[3] However, reduction in fertility is possibly related to Se deficiencies, even if the target organ for Se action is, at present, unclear.[1,9] Se has been linked to function in epidemiological studies but no biochemical pathway has been identified. It has been demonstrated that nutrient restriction and/or Se level in the maternal diet affect cell proliferation in follicles, blood vessels, and stromal tissues in ovine fetal ovaries[10] and Se deficiency has additionally been shown to lead to degeneration of ovaries and atresia of follicles in rats.[11] There are many factors which control oocyte growth and follicular maturation, including: nutritional imbalances; hormonal disturbances; and, physical conditions of the microenvironment, of which oxidative stress is an important component.[4] Elevated ROS levels, which disrupt the peritoneal fluid balance of oxidants and antioxidants, are thought to establish infertility in women where other etiological factors are not identified.[12]

Ovarian function has been extensively studied in bovine species. Follicles are ordinarily categorized according to their stage of growth as: primordial follicles, containing an oocyte surrounded by one layer of flattened pregranulosa cells; after activation as primary follicles, with one layer of cuboidal granulosa cells; as preantral follicles with increasing layers of granulosa cells; and, after formation of a follicular fluid-filled antrum and a specialized thecal

layer, as antral follicles. At the antral stages the oocyte is surrounded by specialized cells referred to as cumulus cells. Granulosa cells support the growth of the oocyte, and in late follicular development secrete estrogens which are essential for normal reproductive function. Most ovarian follicles do not mature to ovulation but rather undergo atresia;[7] characterized in the first instance by apoptosis of granulosa cells. In the current study, the terms 'small' and 'large' are used to describe antral follicles which are less than 4 mm and greater than 10 mm, respectively.

During a follicular growth wave, an increase in follicle-stimulating hormone (FSH) levels induces the further growth and differentiation of a cohort of follicles beyond 4 mm in diameter. From this cohort, only one follicle will be selected as the dominant follicle and continue to grow beyond 8 mm. The dominant follicle can ovulate, whereas all other follicles undergo atresia.[13,14] Cohort follicles, therefore, require elevated concentrations of FSH while the dominant follicle, in contrast, has a higher FSH responsiveness, demonstrated by its enhanced growth and estradiol synthesis in a low FSH environment.[15] At this point the dominant follicle requires frequent stimulation by luteinizing hormone (LH) to continue differentiation leading up to ovulation,[16] after which the remnants of the follicle wall transform into the corpus luteum. Understanding the mechanisms by which a single follicle is selected for dominance and understanding the cellular mechanisms that permit the transition from the FSH- to the LH-dependent developmental stage in the dominant follicle is essential, as ovarian conditions resulting in anovulation are one of the major causes of infertility in both bovine and human species.[17,18,19]

New technologies, such as three-dimensional ultrasonography and magnetic resonance imaging, ultrasound-based biomicroscopy and synchrotron-based techniques have the potential to enhance our real-time picture of ovarian function to the near-cellular level.[20] The use of synchrotron light in medical imaging has been rarely used to image ovarian tissue of any species nor have the mechanisms of Se distribution in mammals been comprehensively investigated, excluding a study on the role of glutathione peroxidase 4 (GPX4) in sperm maturation in murine species.[21,22,23] The ability to probe the *in situ* bioaccumulation of trace metals to a specific ovarian structure or cell type has the potential to provide unprecedented insights into the biochemistry of this organ. We therefore undertook X-ray fluorescence imaging of bovine ovaries and focused on Se. With additional studies we identified the major selenoprotein in the ovaries and identified a possible role of this selenoprotein.

Materials and methods

Sample collection for XRF analysis

Bovine ovaries were sourced from T&R Pastoral's abattoir, Murray Bridge, South Australia. Ovaries were collected from Bos taurus non-pregnant heifers (n = 32) and collected in pairs into ice-cold Hank's Balanced-Salt Solution (HBSS) and transported on ice to the laboratory. For XRF imaging sections were cut into halves longitudinally, frozen and stored in O.C.T. compound (ProSciTech, Thuringowa, QLD, Australia) at -80°C until sectioning.

Sample collection for ICP-MS analysis

A pair of bovine ovaries was collected from a non-pregnant heifer at T&R Pastoral's abattoir, Murray Bridge, South Australia and subsequently dissected to obtain tissue samples representative of the corpus luteum and follicle wall (granulosa and thecal cells). The first ovary was dissected to obtain three representative samples of the corpus luteum (Stage III). The second ovary was dissected to obtain theca/granulosa cells from all of its follicles with the first sample containing the thecal/granulosa layers from a single 9 mm follicle and the second sample containing the pooled thecal/granulosa cell layers from the four remaining follicles: 6 mm, 7 mm, 7 mm and 10 mm. The samples were weighed, the wet weight recorded, and then freeze dried for a period of six hours, after which the dry weights were recorded.

Histology and preparation of tissue for XRF analysis

Each O.C.T. embedded ovary was sectioned at a thickness of 30 μm for XRF analysis and adjacent 6μm sections for H&E staining. Sectioning was performed on a CM1800 Leica cryostat (Adeal Pty. Ltd., Altona North, Vic, Australia). Each XRF section was transferred on Ultralene thin film (SPEX SamplePrep, New Jersey, USA) affixed to a 24 × 36 mm photographic slide frame with stainless steel tweezers and an artist grade Filbert type synthetic paint brush. Tissue was then dried in a desiccator under vacuum overnight and stored in a desiccator until analysis. Sections intended for H&E staining were mounted on glass slides treated with 0.01 % poly L-ornithine hydrobromide (Sigma-Aldrich Pty. Ltd., Castle Hill, NSW, Australia), and stored at -20°C until use.

Classification of follicles

The H&E stained follicle sections were observed by light microscopy and assessed as healthy or atretic based upon the morphology of the membrana granulosa and the percentage of pyknotic nuclei, as previously described.[24,25]

X-ray fluorescence imaging

The distribution of elements throughout selected 30 μm bovine ovarian sections was mapped at the XFM beamline at the Australian Synchrotron, Clayton, VIC, Australia. An incident beam of 15.75 keV X-rays was chosen to induce K-shell ionization of elements with atomic numbers below 37 (Z ≤ Rb), while providing adequate separation of the Rayleigh and Compton peaks from the elemental fluorescence of interest, i.e. Se. The incident beam was focused to a ~2 μm (fine scans) or ~6 μm spot [coarse scans (full-width at half maximum)] using a Kirkpatrick–Baez mirror pair and specimens were fly-scanned through X-ray focus. The resulting XRF was collected in event-mode using the low-latency, 384-channel Maia XRF detector (positioned in the backscatter geometry) and the full XRF spectra were used to reconstruct elemental maps of the specimen using a virtual pixel size of 2 or 6 μm (fine and coarse scans, respectively).

The effective per pixel dwell times for the fine and coarse scans were 7.81 ms or 2.44 ms, respectively and the largest scan depicted in this manuscript was 1291 × 1579 pixels in size. Single element

foils of Mn and Pt (Micromatter, Vancouver, BC, Canada), were scanned in the same geometry and used as references to establish elemental quantitation. Deconvolution of the Maia data was performed using the GeoPIXE v6.5h (CSIRO, Australia) that incorporates a linear transformation matrix to perform spectral deconvolution.[26] Spectra were calibrated using the metal foil measurements, and corrections made for self-absorption in the sample, absorption in air, and the efficiency response of the detector.[27] The detected X-ray photons from each pixel were related to calculated-model fluorescence X-ray yields for an assumed specimen composition and thickness. The composition and thickness of the Ultralene film was known from the manufacturer's specifications and the composition and average density typical of dried organic material ($C_{22}H_{10}N_2O_4$ and 1.42 g cm^{-3} respectively), was used to model the tissue. Absorption effects for XRF from the lowest atomic number element relevant to this study (Ca Kα) were negligible for this specimen type.

ICP-MS of granulosa and thecal cells and corpus luteum

Three samples along with two samples of NIST 1577b bovine liver standard (Gaithersburg, MD, USA) were taken to CSIRO's Land and Water Laboratory (Glen Osmond, SA, Australia) for microwave assisted acid based digestion. Briefly, the specimens were cold digested overnight in 7 mL of concentrated nitric acid (Fisher Scientific AR Grade 70%, VIC, Australia) and 3 mL of concentrated H_2O_2 (Chem Supply AR Grade 30%, SA, Australia). All solutions underwent a standardized 105 min digestion in a laboratory grade microwave, with the temperature gradually increasing up to 180°C, and then maintained at this temperature to ensure complete digestion. Following adequate cooling the resultant digests were diluted up to 50 mL using milliQ water.

The digests were then run neat through the Solution ICP-MS instrument (Agilent 7500cs with Octopole Reaction System, Mulgrave, VIC, Australia) with detection of the second most abundant isotope of Se, namely ^{78}Se, avoiding interference from ^{40}Ar$_2$. Calibration standards made up from multi elemental solution were run prior to the bovine samples and the resultant curve produced a correlation coefficient of 0.9993 for ^{78}Se. Concentrations were reported in mg/kg relative to the dry weight of material.

Microarray analysis

Previously collected microarray data,[28] deposited in the GEO under accession numbers GSE39589 and GSE49505, were examined to compare the values of the mean intensity for the expression of 19 different selenoproteins in both the theca and granulosa cells of small healthy, large healthy, and small atretic bovine ovaries (Supplementary Data Set 2). Based on analysis of the XRF data it was apparent that the Se species of interest was localized to the granulosa cells, and of markedly higher concentrations in large healthy follicles. Supplementary Table 1 provides a summary of the selenoproteins considered for further analysis with a detailed legend indicating the most likely candidates for the species imaged via XRF.

A shortlist of potential Se proteins up-regulated in the granulosa cells of healthy large follicles was identified from the microarray analysis as being: GPX1, GPX3, SEP15, VIMP, SELK, SELT, SELM, and SEPHS2. This was narrowed further by eliminating those selenoproteins for which the up-regulation

was minor (indicated in *italics*) in both groups (SEP15) or minor in one group and moderate (indicated with <u>underlining</u>) in another (SELK, SELT and SEPHS2), leaving: GPX1, GPX3, VIMP and SELM.

RNA extraction and cDNA synthesis

Total RNA was extracted from granulosa cells using Trizol reagent as per the manufacturer's instructions. The quantity of total RNA was determined by spectrophotometry (Absorbance at 260 nm; 1000V 3.3 spectrophotometer, NanoDrop Technologies Inc., Wilmington, DE, USA). Two micrograms of RNA was DNase-treated (DNA-free, Ambion, Supplied by Applied Biosystems, Melbourne, VIC, Australia). Complementary DNA (cDNA, 20µl) was synthesized according to the manufacturer's instructions using 500 ng random hexamers (GeneWorks, Adelaide, SA, Australia), 10 nmol dNTP mix, 20U RNaseOUT and 200U of Superscript III RT (Life Technologies, Mulgrave, VIC, Australia). The RNA, random hexamers and dNTPs were pre-incubated at 65°C for 5 min before adding to a reaction mixture including 4µl 5× First Strand Buffer, 1µl of 0.1M dithiothreitol, 4U RNAseOUT (Life Technologies) and enzyme, with further incubation at 50°C for 60 min followed by 70°C for 15 min to inactivate enzymes prior to PCR.

Quantitative real time RT-PCR

To identify the Se species imaged in the granulosa via XRF, quantitative real time RT-PCR for GPX1, GPX3, VIMP and SELM was performed on granulosa cells derived from small healthy (n = 5), small atretic (n = 5), and large healthy (n = 5) follicles. All primers were designed using Primer Express software (Life Technologies) (Supplementary Table 2). Expression for each gene was normalized to the expression of the house-keeping gene 18S rRNA and our results are expressed as fmol of mRNA per nmol of 18S rRNA. The PCR was carried out using a Corbett Rotor Gene 6000 (Qiagen, Hilden, Germany) with 2 µl of diluted cDNA in a SYBR Green Master Mix (Applied Biosystems, Foster City, CA, USA). Each run was performed with water blanks and non-reverse transcribed RNA as negative controls. Samples were amplified in duplicate with an initial denaturation at 95°C for 10 min, followed by 40 cycles of 2-step amplification at 95°C for 15 s and 60°C for 60 s. The concentration of each target was generated from the Ct value and standard curve (amplification efficiency > 0.9), and was normalized to the concentration of 18S ribosomal RNA in each sample (calculated by the Ct and standard curve for 18S). For each PCR reaction, melt curve analysis was conducted to confirm the correct product was amplified based on initial gel electrophoresis and DNA sequencing.

Statistical analyses

All statistical calculations were performed using SPSS version 20 (SAS Institute Inc., Cary, NC, USA). For the ICP-MS data, results are presented as means ± standard deviation. To compare the level of gene expression between granulosa cell groups Kruskal-Wallis one way ANOVA with post hoc Mann-Whitney tests were employed.

Immunohistochemistry

Portions of the previously collected bovine ovaries were used for localization using an indirect immunofluorescence method. Frozen tissue sections were dried under vacuum for 5 min, fixed in 10% neutral buffered formalin for 5 min, and rinsed three times for 5 min in hypertonic phosphate buffered saline (PBS) (10 mM sodium/potassium phosphate with 0.274 M NaCl and 5 mM KCl, pH 7.2) before treatment with blocking solution (10% normal donkey serum [D-9663; Sigma Chemical, St. Louis, MO, USA] in antibody diluent containing 0.55 M NaCl and 10 mM sodium phosphate, pH 7.1) for 30 min at room temperature. The primary antibodies used were polyclonal rabbit anti-human VIMP (1:100 dilution; NBP1-89558; Novus Biologicals distributed by Sapphire Bioscience Pty. Ltd., Waterloo, NSW, Australia) in combination with rat anti-mouse Perlecan A7L6 (1:100 dilution; Millipore Pty. Ltd., Kilsyth, VIC, Australia). The ovarian sections were incubated with the primary antibodies overnight at room temperature. After three washes with PBS the ovarian sections were incubated for 2 h at room temperature with FITC-conjugated AffiniPure donkey anti-rat (#712-096-153) and biotin-SP-conjugated AffiniPure donkey anti-rabbit IgG (#711-065-152) and after three washes with PBS, subsequently incubated for 1 h at room temperature with Cy3-conjugated streptavidin (#016-160-084). All secondary antibodies and conjugated streptavidins were purchased from Jackson ImmunoResearch Laboratories (distributed by Abacus ALS Australia, Brisbane, QLD, Australia) and used at 1:100 dilutions. Finally, sections were treated with the nuclear stain 4',6'-diamidino-2-phenylindole dihydrochloride (DAPI) solution (Molecular Probes, Eugene, OR, USA) to identify cell nuclei. Coverslips were attached with mounting medium for fluorescence (S3023; Dako, Carpinteria, CA, USA) and photographed with an Olympus BX50 microscope (Olympus, Tokyo, Japan) with an epifluorescence attachment and a Spot RT digital camera (Diagnostic Instruments, Sterling Heights, MI, USA).

Protein extraction and Western immunoblotting

Following collection (previously described) the follicles were dissected from each ovary and the diameter measured. A small piece of the follicle wall, approximately 1 mm^3, was removed and fixed in 2.5% glutaraldehyde in 0.1 M phosphate buffer (pH 7.25) for subsequent classification of follicle health status.[29] The granulosa cells were removed from the remainder of the follicles. The HBSS without Mg^{2+} and Ca^{2+} containing the granulosa cells was centrifuged at 500 x g for 7 min at 4°C, the medium was removed by aspiration and the cells washed twice in PBS pH 7.4, and then frozen at -80°C.

Following fixation overnight, the follicle wall portions of each follicle were rinsed several times with 0.1 M PBS, pH 7.25, post-fixed in 2% (v/v) aqueous osmium tetroxide for 1 h at 4°C and embedded in epoxy resin as described previously.[30] For light microscopic examination, 0.5 μm thick epoxy sections were cut using a glass knife and a Richert-Jung Ultracut E ultramicrotome (Leica Microsystems Pty Ltd., VIC, Australia), stained with 1% (w/v) aqueous methylene blue and examined using an Olympus BX50 microscope (Olympus Australia Pty Ltd., Mt Waverly, VIC, Australia). Healthy and atretic follicles were identified as described previously.[24, 31] wherein healthy follicles had less than 5 % apoptotic granulosa cells and atretic follicles had more than 5 % apoptotic granulosa cells. Only

granulosa cells from healthy follicles were examined for expression of GPX1.

For Western blotting a total of nine granulosa cell samples (small healthy follicles, n = 4, 3-5 mm and large healthy follicles, n = 5, 13.5 mm ± 0.8 mm) from nine different animals were used. Total protein was extracted from samples using RIPA buffer [1 % NP-40, 1 % sodium deoxycholate, 0.1 % sodium dodecyl sulfate (SDS), 0.15 M sodium chloride, 50 mM Tris-hydrochloric acid and 1 mM ethylenediaminetetraacetic acid (EDTA)] containing 1 μl of protease inhibitor cocktail (Sigma Aldrich, St Louis, MO, USA) per 100 μl . Cells in RIPA buffer were disrupted with a 5 s pulse at 3500 rpm using a MO BIO Powerlyzer 24 Homogenizer (MO BIO, Carlsbad, Ca, USA). The homogenates were centrifuged at 10 000 g for 10 min to pellet insoluble material and the supernatants were taken for analysis. Proteins were quantified using the Bradford method (Bio-Rad Laboratories, Hercules, CA, USA) and 20 μg of protein for each sample were separated on a 4-15 % gradient SDS-PAGE gel and then transferred overnight at 4°C to polyvinylidene difluoride (PVDF) transfer membrane (Amersham Hybond TM-P, GE Healthcare, Buckinghamshire, UK), at a constant voltage (33 V). All washes and incubations of the membranes were performed at room temperature. The PVDF membrane was washed three times for 5 min with Tris-buffered saline containing 0.1 % Tween-20 (TBS-T; 50 mM Tris, 100 mM sodium chloride, pH 7.5, Sigma-Aldrich, St Louis, MO, USA). Non-specific binding was inhibited by incubating with 10 % skim milk in TBS-T for 1 hr. For GPX1 detection, the membranes were then incubated with the rabbit anti-GPX1 antibody (ab22604, Abcam, Cambridge , UK) for 2 h at a 1 in 1000 dilution in 10% skim milk/TBS-T. After incubation, membranes were again washed and then incubated (for 1 h) with a goat anti-rabbit secondary antibody conjugated with horseradish peroxidase diluted 1:10 000 in 10% skim milk/tris-buffered saline and Tween (TBS-T), then washed five times (3 x 30 s, 1 x 5 min and 1 x 10 min wash) with TBS-T. For actin detection, membranes were incubated for 2 h with monoclonal anti-β-Actin−peroxidase antibody (A3854, Sigma Aldrich, St. Louis, MO, USA) diluted 1:20 000 in 10% skim milk/TBS-T. The membranes were then washed five times (3 x 30 s, 1 x 5 min and 1 x 10 min wash at room temperature) in Tris-buffered saline with 0.5% Tween-20 and 0.1% SDS. All membranes were finally incubated with ECL ClarityTM Western blotting detection reagent for 5 min and exposed to Amersham HyperfilmTM ECL (GE Healthcare, Buckinghamshire, UK) for protein detection by chemiluminescence.

IVF and Human Cumulus Cells

Details of the collection of human cumulus cells were as conducted previously, excepting that the RNA isolation was different.[32] Ethical approval for the use of human samples was obtained from the Women's and Children's Hospital Human Research Ethics Committee, Adelaide, Australia and the Repromed Scientific Advisory Committee, Adelaide, Australia. Written consent for the use of cumulus cells for research was obtained from thirty patients undergoing routine IVF/ICSI with Single Embryo Transfer (SET) using their own gametes at Repromed, Dulwich, South Australia. Patients with clinical indications of polycystic ovary syndrome were not included in this study. All patients were stimulated using a long down-regulation protocol involving the administration of a Gonadotropin Releasing Hormone analog (Nafarelin (Synarel), Organon, Australia) confirmed with blood estrogen levels

below 0.2 nM/L. Recombinant FSH (Gonal-F, Serono, Sydney, Australia or Puregon, Organon, Sydney, Australia) was administered for 9-12 days, monitored by ultrasound, until the lead follicle was a size of 18 mm. Patients were then given 5,000 IU human Chorionic Gonadotropin (Pregnyl, Organon, Sydney, Australia) 36 h later. Cumulus-oocyte complexes from follicles greater than 14 mm were collected using transvaginal ultrasound and a 17-gauge needle.

Culture was performed at 37°C, 6% CO_2, 5% O_2, 89% N_2, in a humidified atmosphere, with manipulations being performed at 37°C, 6% CO_2. Cumulus-oocyte complexes were washed in glucose-supplemented (2.5 mM glucose) GFERT-plus medium and stored in 1 mL of the same medium for 3 h post-oocyte collection for both IVF and ICSI inseminations. The outer layers of cumulus cells were trimmed with a 30 gauge needle and collected individually prior to insemination and stored at -80°C. Oocytes undergoing ICSI were exposed to 75IU Hyaluronidase (Hyalase®, Aventis Pharma Pty Ltd, Lane Cove, Australia) in glucose supplemented GFERT and then ICSI performed in G1.3 plus medium and cultured singly in 10 µL drops of the same medium under oil for 16-18 h. Oocytes undergoing IVF had the inner layers of cumulus left intact and were co-incubated with 1,000 motile sperm in 10 µL drops of glucose-supplemented GFERT-plus medium under oil for 17-19 h. All oocytes were cultured individually, fertilization was assessed 16-19 h post-insemination, and embryos with two pronuclei continued culture individually in 10 µL drops of G1.3 Plus medium under oil for the next 48 h. These embryos were then washed thoroughly through G2.3 Plus medium and cultured for another 48 h before being transferred to fresh G2.3 medium for the final 24 h of culture.

Embryo transfers were performed on days 2/3 or days 4/5 for extended culture. Standardised morphology assessments of the day 2 embryo quality score was used to select embryos for transfer and in all cases a single highest morphological quality embryo was transferred. On day 2 after fertilization cleavage stage morphology scoring was based on the number of cells, the degree of fragmentation, and the presence of multinucleated cells. Clinical pregnancy was determined by the presence of a fetal heart beat 6 weeks following embryo transfer. Live birth outcomes were obtained from the obstetrician in charge of the patient care. Obstetricians provided delivery dates, birth weights, sex and whether there were any maternal or neonatal interventions or complications.

Isolation of RNA from Human Cumulus Cells and Real Time RT-PCR

All reagents for RNA extraction, cDNA synthesis and real-time PCR were purchased from Life Technologies (Waverley, Vic, Australia) unless otherwise stated. Cumulus cell RNA was extracted using Trizol, as per the manufacturer's instructions with the inclusion of 7.5 µg of glycoblue during precipitation overnight at -20°C. Total RNA was eluted in 20 µl of elution buffer then treated with 2 U of DNase I for 30 min at 37°C to remove genomic DNA. Complementary DNA (cDNA) was synthesized from 30–300 ng total RNA using random hexamer primers (Geneworks, Adelaide, Australia) and Superscript III reverse transcriptase. Taqman Gene Expression Assays, containing specifically designed primers and a FAM-labelled probe, were purchased for the human genes MRPL19 (# Hs00608519_m1) and GPX1 (# Hs00608519_m1). Real-time RT-PCR was performed in duplicate for each sample on the Corbett Rotor Gene 6000 (Corbett Life Science, Qiagen). In each reaction, cDNA (equivalent to 5 ng of total RNA), 0.2 µl

of Taqman assay, and 5 µl of Taqman master mix were added, with H_2O added to make a final volume of 10 µl. PCR cycling conditions were 95°C for 10 min, followed by 40 amplification cycles of 95°C for 15 sec and 60°C for 1 min. Controls included omission of the cDNA template or RT enzyme in otherwise complete reaction mixtures; each showing no evidence of product amplification. The expression of GPX1was normalized to the housekeeping gene MRPL19 by calculating the ratio of $2^{-\Delta Ct}$. The values obtained for the pregnant and non-pregnant groups were compared statistically by a two-tailed Student's t-test assuming equal variance in SPSS v 20.

Results

XRF imaging of bovine follicles

A pilot study which collected XRF elemental distribution images for an entire section of a single ovary led to the hypothesis that Se was actively mobilized to the thecal/granulosa cell region of large follicles (Fig. 1). X-ray fluorescence imaging was subsequently utilized to image key structural features within bovine ovarian cross sections of 45 different animals including: granulosa and thecal cells of primordial, primary, preantral and antral follicles, including healthy follicles and those undergoing atresia; corpora lutea at different stages of development [Stages I (early) through to IV(regressing) [33]]; corpus albicans (regressed corpora lutea); arterioles; vessels; and, capillaries. Qualitative elemental distribution trends were identified for Fe, Zn and Se, with all ovaries showing strong signals and distinct localizations of the first two elements. Zn was consistently present throughout the ovarian tissue but elevated around arterioles and capillaries, while Fe was concentrated in the corpora lutea and in blood vessels (unpublished observations).
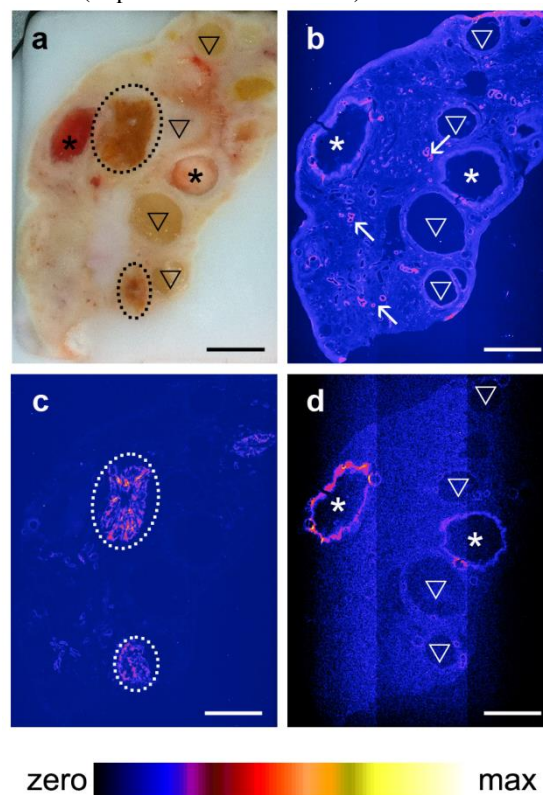
Fig. 1 Distribution of Zn, Fe and Se in a bovine ovarian section as imaged by μ-XRF. Comparison with the adjacent fresh frozen tissue (a) indicates that regions of high Zn (b, pink) intensity correspond to arterioles and capillaries; high Fe (c, pink) correspond to corpora lutea; and, high Se (d, pink) is localized to the granulosa cell layers of the two largest healthy follicles. Maximum pixel values for Zn, Fe, and Se are 63.7, 329 and 3.61 ppm, respectively. ▽ indicates atretic follicle; * indicates healthy antral follicle; ---- indicates corpus luteum; ⤶ indicates vasculature. Scale bar: 4 mm.

Se was found to be localized to the granulosa cell layer of large healthy follicles (Fig. 2b), with a regularity and intensity that was not observed in the small (< 4 mm), small-medium (4-8 mm), medium-large (8-10 mm) or, large atretic counterparts (Fig. 2d). Se signals in large follicles were observed in 100% of healthy (n = 10) whereas only 30% of atretic follicles (n = 10) showed Se. No Se signal was observed in large regressing follicles (n = 2) (Supplementary Data Set 1).
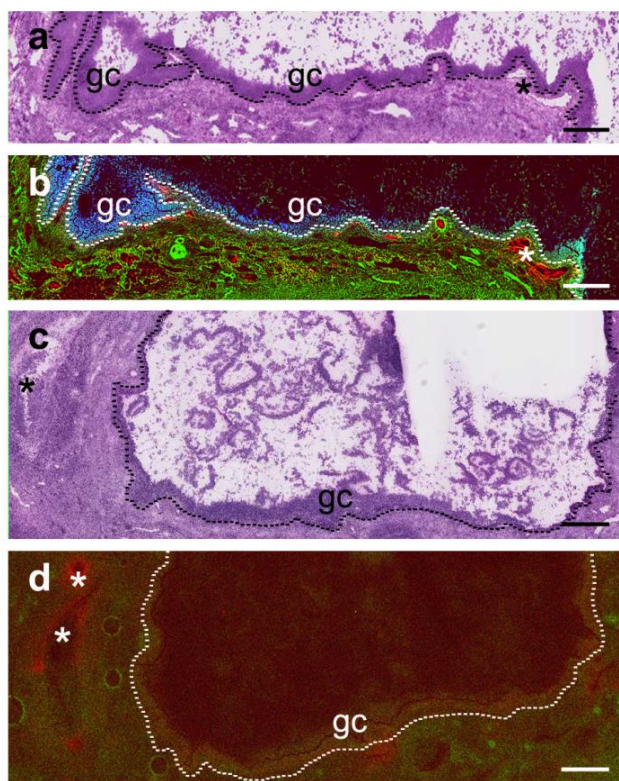
Fig. 2 Localization of Zn, Fe and Se in large antral follicles. (a) H&E stained serial section of a 15 mm diameter healthy follicle. (b) The corresponding RGB image has been generated from XRF elemental distribution maps and depicts the distribution of Zn (green), Fe (red) and Se (blue). The virtual pixel size for this fine scan was 2 μm with an effective per pixel dwell time of 7.81 ms. Maximum pixel values for Zn, Fe, and Se are 22.4, 189 and 5.19 ppm, respectively. (c) H&E stained serial section of an 11 mm atretic follicle. (d) The corresponding RGB image has been generated from XRF elemental distribution maps and depicts the distribution of Zn (green) and Fe (red). No Se was detected. Maximum pixel values for Zn and Fe are 87 and 343 ppm, respectively. The virtual pixel size for this fine scan was 5 μm with an effective per pixel dwell time of 2.44 ms. * indicates vasculature; -----

indicates the separation between granulosa layer and thecal layer; gc indicates granulosa cells. Scale bar: 500 μm.

Quantification of Se using ICP-MS

In order to validate the elevated Se levels observed via XRF imaging a pair of bovine ovaries was collected from a non-pregnant heifer and subsequently dissected to obtain samples representative of the corpus luteum (n = 3) and the follicle wall (granulosa and thecal cells) (n = 2). National Institute of Standards and Technology (NIST) bovine liver (1577b) was used as a concentration standard. Granulosa cells alone would have provided an inadequate mass for digestion and thus the whole follicle wall (theca and granulosa layers) was dissected. All samples were freeze dried and subjected to microwave assisted acid based digestion prior to solution-phase ICP-MS. The concentration of Se determined in the NIST bovine liver (1577b) was found to be 0.8 ± 0.03 ppm which lies within the range of certification. The mean Se concentration for the corpora lutea samples was 2.6 ± 1.3 ppm as compared with the mean experimentally determined concentration for the follicle wall of 26 ± 5.0 ppm. This result supports the qualitative XRF observation that large healthy follicles contain a Se rich component as opposed to the corpora lutea, for which this element was not detected.

Analysis of microarray data

Previously collected microarray data, deposited in the Gene Expression Omnibus (GEO) under accession numbers GSE39589 and GSE49505,[28] was examined to identify selenoproteins candidates (Supplementary Data Set 2) which might explain the high Se levels observed in the XRF and ICP-MS experiments. We identified four potential candidates which were differentially expressed between small and large healthy follicles, and small atretic and large healthy follicles: GPX1, GPX3, VIMP and SELM (Supplementary Table 1).

PCR of granulosa cDNA

Quantitative RT-PCR for *GPX1*, *GPX3*, *VIMP* and *SELM* in granulosa cells from small healthy (n = 5) and atretic (n = 5), and large healthy (n = 5) follicles showed only a significant up-regulation of *GPX1* in large healthy follicles compared to small healthy or atretic follicles ($P < 0.05$) (Fig. 3).

Immunohistochemical localization of VIMP in ovarian sections

Immunohistochemistry for the selenoprotein VIMP in large bovine follicles showed that it is expressed in the granulosa cell layer of large healthy follicles (Fig. 4b) and to a lesser extent in the granulosa cell layer of large atretic follicles (Fig. 4d). Furthermore, VIMP is also expressed in the thecal cell layer of large healthy follicles.

Detection of GPX1 in different follicular cell types

Fig. 5 depicts Western immunoblotting of granulosa cell proteins. Fig. 5a and b indicates that none of the small follicle granulosa cell samples had measurable levels of GPX1, while three of the five large follicle samples were positive for GPX1.

GPX1 in Cumulus Cells from Human Oocytes

Expression of GPX1 was found to be significantly higher in cumulus cells isolated from cumulus oocyte complexes of human follicles where the oocyte yielded a successful pregnancy (Fig. 6).
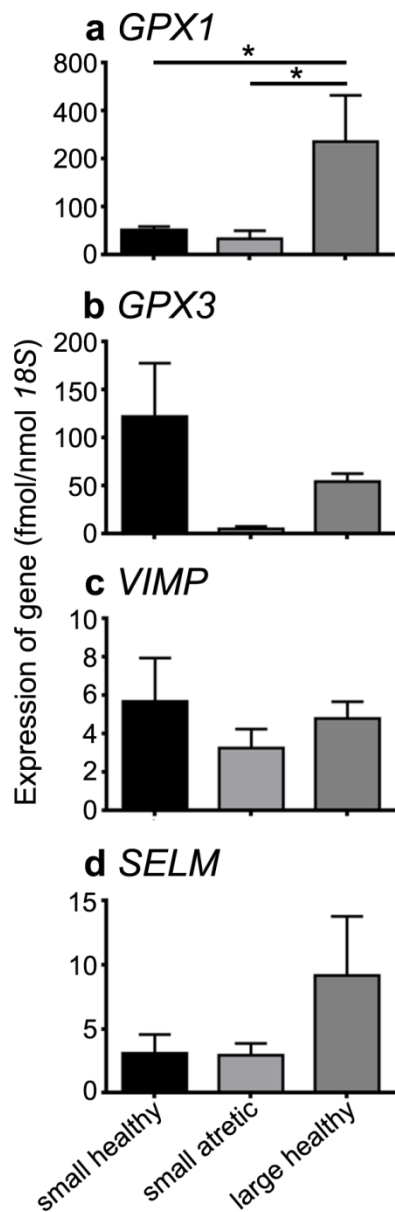
Fig. 3 Mean levels of selenoprotein mRNA. Mean levels ± SEM of (a) GPX1, (b) GPX3, (c) VIMP and (d) SELM mRNA relative to 18S ribosomal RNA in granulosa cells derived from small healthy, small atretic and large healthy follicles (n = 5 follicles per group). * denotes a statistically significant difference between groups ($P < 0.05$).
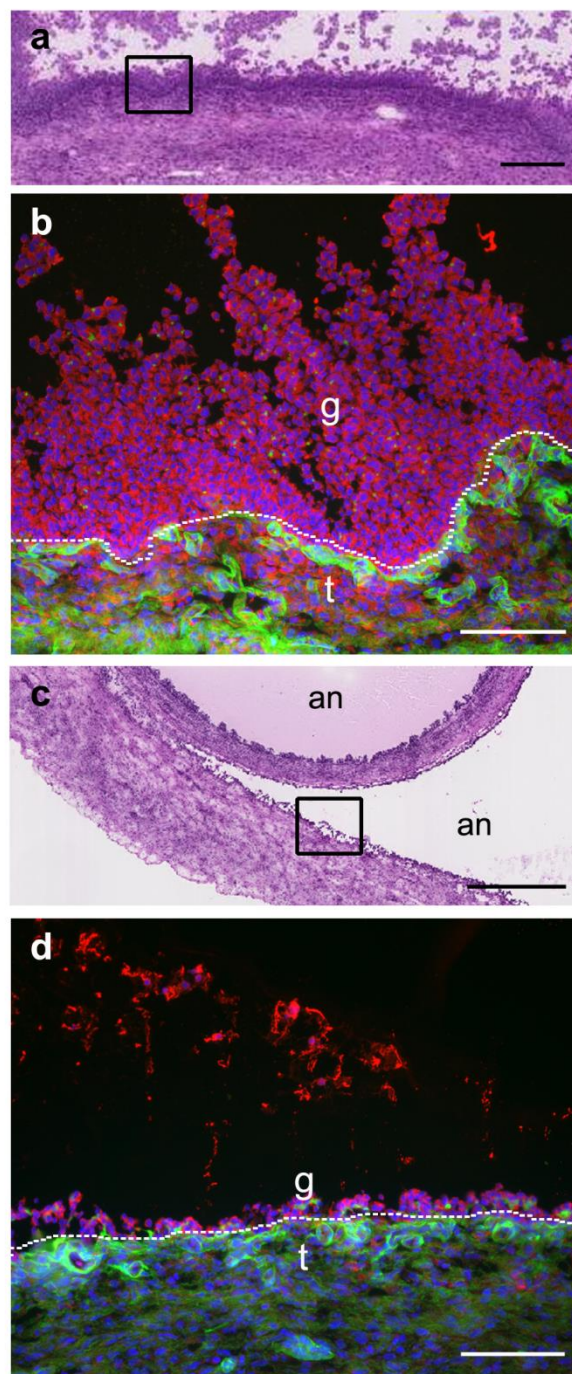
Fig. 4 Immunostaining for VIMP in large follicles. (a) H&E of serial section of a large 15 mm diameter healthy follicle. The square shows the area shown in (b). Scale bar: 250 µm. (b) VIMP (red) is localized to the granulosa cell (g) layer and the thecal cell (t) layer. an indicates the antral cavity. The basal lamina (------) separating the two cell layers is stained for perlecan (green). Nuclei are counterstained with DAPI (blue). Scale bar: 100 µm. (c) H&E of continuously followed serial section in a large 17 mm atretic follicle. The square identifies the area shown in (d). Scale bar: 500 µm. (d) VIMP (red) is localized to the granulosa cell (g) layer and the thecal cell (t) layer. The basal lamina (------) separating the two cell layers is stained for perlecan (green). Scale bar: 100 µm.
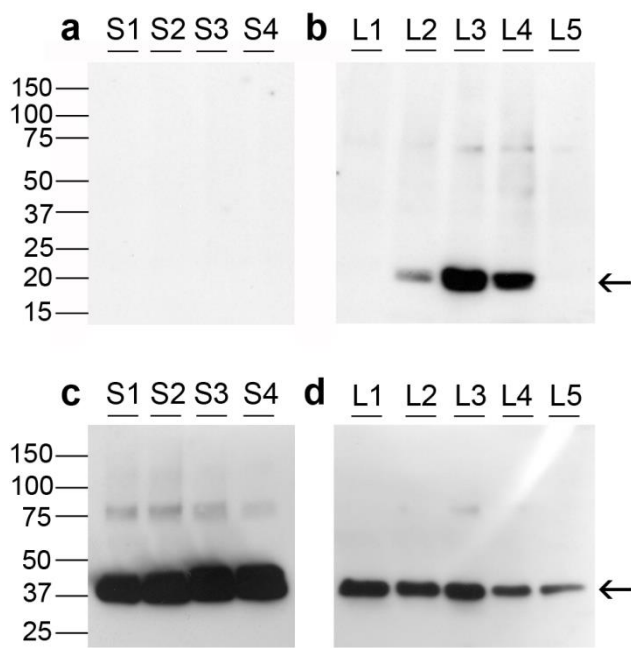
Fig. 5 Western immunoblotting of GPX1 in granulosa cells from small and large healthy follicles. Each lane marks granulosa cell extracts from individual follicles. (a) GPX1 expression (marked with arrow, 20 kDa) in granulosa cells of small healthy follicles (n = 4, 3-5 mm). (b) GPX1 expression (marked with arrow, 20 kDa) in granulosa cells of large healthy follicles (n = 5, 13.5 mm ± 0.8 mm). (c) Corresponding actin expression (marked with arrow, 37 kDa) in the same blot as (a). (d) Actin expression (marked with arrow, 37 kDa) in the same blot as (b).
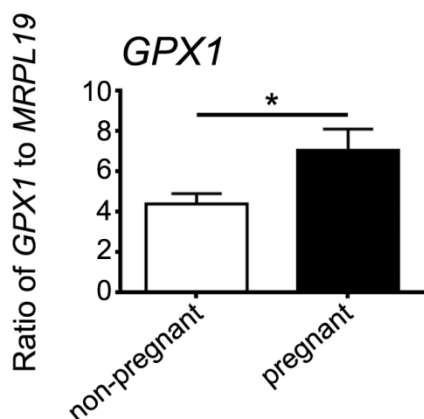
Fig. 6 Expression of GPX1 in cumulus cells isolated from cumulus-oocyte complexes of oocytes in an IVF/ICSI program that upon embryo transfer either did (n = 12) or did not (n = 18) result in a pregnancy. *denotes a statistically significant difference between groups (P < 0.05).

Discussion

Expression of GPX1 is influenced by nutritional status

Here we present the first XRF imaging of mammalian ovaries showing that Se is consistently localized to the granulosa cells of large healthy follicles. Subsequent experiments including quantitative real time RT-PCR and Western immunoblotting

identify the source of the Se to be the selenoprotein GPX1, a ubiquitous homotetrameric cytosolic enzyme expressed by many cell types in mammals.[3, 34] Expression of GPX1 was examined in cumulus cells isolated from cumulus-oocyte complexes of oocytes undergoing IVF/ICSI and found to be elevated where the oocytes yielded a successful pregnancy.

GPX1 is abundant in the liver and erythrocytes, with its concentration being dependent on the nutritional Se status. It is also one of the most highly sensitive selenoproteins to change with Se status. The levels of mRNA and protein are dramatically reduced under low Se conditions.[35] It should be noted however that previous studies have shown the extent of GPX1 regulation varies from organ to organ under Se deficit.[36] In addition to Se status, other factors including oxidative stress influence the expression of GPX1. Synthesis of GPX1, GPX3 and thioredoxin reductase 1 (TR1) are also up-regulated during thyroid hormone synthesis, providing the thyrocytes with considerable protection from peroxidative damage.[3]

Selenoproteins such as GPX may combat oxidative stress during follicular development

Whilst the role of Se in regulation of ovarian function in the fetus is unclear,[10] in adult ovaries it has been demonstrated that Se intake may modulate granulosa cell proliferation and estradiol-17β synthesis in vitro.[9,10,37] Moreover, its effect could be mediated, at least in part, through an inhibition of nitric oxide. It has been shown that culture of preantral follicles in the presence of sodium selenite increases GPX activities and decreases ROS levels, thereby improving the development rate of mouse follicles in vitro.[4] With regard to the theca, evidence exists to suggest that antioxidants such as Vitamin E and ebselen are capable of inducing apoptosis in rat ovarian theca-interstitial cells.[38] This finding may have important clinical relevance to Polycystic Ovary Syndrome (PCOS), a condition associated with excessive growth and activity of theca-interstitial cells.[38] This condition affects 5-10% of women in the reproductive age and there is emerging evidence that chronic low-level inflammation is often present in women with PCOS with the possible effect of increasing oxidative stress.[39] A recent study of Turkish women with PCOS found that the plasma Se levels of these women were significantly lower than the control groups suggesting that Se may play a role in the pathogenesis of this condition.[40] These findings should however be contrasted with much earlier research which suggested that inhibition of oxidative stress suppressed apoptosis of granulosa cells in cultured follicles, indicating that effects of antioxidants on apoptosis are cell-type dependent.[38, 41] Exploring the potential link between FSH and glutathione found firstly that the onset of apoptosis in preovulatory follicles is preceded by a rise in follicular ROS and secondly, that treatment with FSH enhances follicular glutathione content and suppresses ROS levels.[7] These studies create a strong case to justify further studies of Se supplementation in women experiencing infertility.

Expression of GPX appears unique to large follicles

The relationship of Se presence with both size of follicle and state of health suggests an important biological role with the most likely function being that the selenoproteins are providing a defense against oxidative stress and inevitable atresia or damage to DNA in the oocyte. In particular the highest levels of Se and GPX1 were observed in granulosa cells of large follicles which are known to express higher levels of cytochrome P450s

(cholesterol side-chain cleavage and aromatase)[42] to enable large dominant follicles to synthesize progesterone and estradiol-17β. Cytochrome P450 enzymes produce superoxide free radical anions and H_2O_2 as part of their mechanisms[43] and hence their up-regulation may constitute an oxidative stress, necessitating the expression of GPX to counter this. In attempting to characterize the regulation of apoptotic death of granulosa cells in dominant bovine follicles during the first wave of follicular development, researchers concluded that the expression of GPX was highest on day 8 relative to days 4 and 6 *in vivo*.[44] The work however makes no specific mention as to the form of GPX identified, making us reluctant to draw comparisons with the findings of our own quantitative real time RT-PCR. Other authors have reported that GPX1 has the highest level of expression in the granulosa cells of the most estrogenic follicle prior to emergence of the dominant follicle and then after emergence the dominant follicle has higher levels than the subordinate follicles.[15] One other study, which used a combination of microarray and quantitative real-time PCR analysis in an attempt to identify differentially expressed genes between largest and second-largest follicles, found GPX3 up-regulation in the dominant follicle, but did not report GPX1 levels.[45] These experimental observations have lead some researchers to hypothesize that follicular oxidative stress-response enzymes are expressed in a stage-dependent manner, since mRNA expression of other anti-oxidative stress enzymes in bovine granulosa cells was increased in atretic dominant follicles relative to healthy dominant follicles.[44-45] The fact that expression of GPX1 was so strongly associated with large follicles in our experiments suggests that this antioxidant could be involved in the signaling process leading to dominance, or that it is simply scavenging the ROS which would otherwise accelerate atresia in competing follicles, or that it protects oocytes from the increasing levels of ROS associated with increasing steroidogenesis in maturing follicles. The latter is supported by our results showing elevated levels of GPX1 in cumulus cells associated with oocytes of greater capacity to yield a pregnancy.

VIMP may play a role in bovine follicular development

Immunostaining for the selenoprotein VIMP showed it is mainly localized to the granulosa cells of large healthy and atretic follicles and also expressed in the thecal layers. This does not contradict the low expression levels seen in the PCR experimentation, but suggests that this selenoprotein provides a small contribution to the strong granulosa cell-specific fluorescence we observe through XRF imaging. Alignment of the VIMP antibody sequence with *Bos taurus* GPX1 shows only 2% sequence identity eliminating the possibility that this antibody is cross reacting with more common members of the GPX family. Taken in conjunction with our gene expression results from the quantitative real time RT-PCR however, we conclude that VIMP is not exclusively localized to the granulosa of large follicles (differences in gene signal expression between small healthy, small atretic and large healthy derived granulosa were not significant), nor is it highly expressed relative to GPX1. This suggests that other selenoproteins are present at background levels throughout the ovarian tissue, but is it only GPX1 that is at sufficiently high concentrations as to be observed through XRF imaging. Additionally the expression of VIMP is not highly dependent on the stage of follicular development.

Computational secondary structure analysis indicates that VIMP is a single transmembrane helix and electron microscopy-assisted immunostaining shows that this species is a plasma and endoplasmic reticulum (ER) membrane protein.[46,47] It has been suggested to participate in the removal of misfolded proteins from the ER lumen for degradation[48] and to protect cells from oxidative damage[49] and ER stress-induced apoptosis.[50] Further experimental results lead to the conclusion that the selenocysteine moiety in the protein may reduce the susceptibility of low density lipoprotein (LDL) to oxidation.[49] A negative association has been found between VIMP and bacterial lipopolysaccharide-induced production of ROS, indicating that VIMP plays an important role in influencing inflammatory response.[51] In a recent attempt to identify its enzymatic function it was concluded that VIMP is primarily a thioredoxin-dependent reductase capable of reducing H_2O_2, but is not an efficient or broad-spectrum peroxidase.[52]

Conclusions

XRF imaging has enabled us to provide possible links between cell specific accumulation of Se and reproductive effects of specific selenoproteins in bovine ovarian tissue.[22] The results presented demonstrate expression of GPX1 (and VIMP) in the granulosa cells of large healthy follicles. Given that a similar distribution of GPX1 was not observed in smaller follicles, our findings indicate that this selenoprotein plays a role in the follicle achieving dominance, thus supporting the gene expression findings of other researchers. The fact that many authors have shown a marked decrease in the expression of the GPX1 gene under conditions of dietary Se reduction leads to the hypothesis that ovarian disorders could, to some extent, be ameliorated by Se supplementation. Our findings could be used to guide epidemiological studies into dietary intake of Se, GPX1 expression in vivo, and the incidence of ovulation disorders.

Acknowledgements

Notes and references

[a] School of Chemistry and Physics, The University of Adelaide, SA, 5005, Australia

[b] Research Centre for Reproductive Health, Discipline of Obstetrics and Gynaecology, School of Paediatrics and Reproductive Health, Robinson Research Institute, The University of Adelaide, SA, 5005, Australia

[c] School of Chemistry, The University of Sydney, NSW, 2006, Australia

[d] Repromed, Dulwich, SA, 5065, Australia

* Corresponding author: School of Chemistry and Physics, The University of Adelaide, SA, 5005, Australia. Email address: hugh.harris@adelaide.edu.au

Metallomics Accepted Manuscript

1. Y. Mehdi, J. L. Hornick, L. Istasse, I. Dufrasne, Selenium in the Environment, Metabolism and Involvement in Body Functions. *Molecules* 2013, **18**. 3292-3311.

2. J. Lu, A. Holmgren, Selenoproteins. *Journal of Biological Chemistry* 2009, **284**. 723-727.

3. G. J. Beckett, J. R. Arthur, Selenium and endocrine systems. *Journal of Endocrinology* 2005, **184**. 455-465.

4. A. Abedelahi, M. Salehnia, A. A. Allameh, D. Davoodi, Sodium selenite improves the in vitro follicular development by reducing the reactive oxygen species level and increasing the total antioxidant capacity and glutathione peroxide activity. *Human Reproduction* 2010, **25**. 977-985.

5. M. A. Reeves, P. R. Hoffmann, The human selenoproteome: recent insights into functions and regulation. *Cellular and Molecular Life Sciences* 2009, **66**. 2457-2478.

6. J. F. Turrens, Mitochondrial formation of reactive oxygen species. *Journal of Physiology-London* 2003, **552**. 335-344.

7. M. Tsai-Turton, U. Luderer, Opposing effects of glutathione depletion and follicle-stimulating hormone on reactive oxygen species and apoptosis in cultured preovulatory rat follicles. *Endocrinology* 2006, **147**. 1224-1236.

8. J. Kohrle, F. Jakob, B. Contempre, J. E. Dumont, Selenium, the thyroid, and the endocrine system. *Endocr. Rev.* 2005, **26**. 944-984.

9. G. Basini, C. Tamanini, Selenium stimulates estradiol production in bovine granulosa cells: possible involvement of nitric oxide. *Domest. Anim. Endocrinol.* 2000, **18**. 1-17.

10. A. T. Grazul-Bilska, J. S. Caton, W. Arndt, K. Burchill, C. Thorson, E. Borowczyk, J. J. Bilski, D. A. Redmer, L. P. Reynolds, K. A. Vonnahme, Cellular proliferation and vascularization in ovine fetal ovaries: effects of undernutrition and selenium in maternal diet. *Reproduction* 2009, **137**. 699-707.

11. M. Grabek, Z. Swies, A. Borzecki, The influence of selenium on the reproduction of rats. *Annales Universitatis Mariae Curie-Sklodowska. Sectio D: Medicina* 1991, **46**. 103-5.

12. A. Agarwal, S. Gupta, L. Sekhon, R. Shah, Redox considerations in female reproductive function and assisted reproduction: From molecular mechanisms to health implications. *Antioxid. Redox Signal.* 2008, **10**. 1375-1403.

13. S. J. Sunderland, M. A. Crowe, M. P. Boland, J. F. Roche, J. J. Ireland, Selection, dominance and atresia of follicles during the estrous-cycle of heifers. *Journal of Reproduction and Fertility* 1994, **101**. 547-555.

14. O. J. Ginther, K. Kot, L. J. Kulick, M. C. Wiltbank, Emergence and deviation of follicles during the development of follicular waves in cattle. *Theriogenology* 1997, **48**. 75-87.

15. M. Mihm, P. J. Baker, L. M. Fleming, A. M. Monteiro, P. J. O'Shaughnessy, Differentiation of the bovine dominant follicle from the cohort upregulates mRNA expression for new tissue development genes. *Reproduction* 2008, **135**. 253-265.

16. Z. L. Liu, R. S. Youngquist, H. A. Garverick, E. Antoniou, Molecular Mechanisms Regulating Bovine Ovarian Follicular Selection. *Mol. Reprod. Dev.* 2009, **76**. 351-366.

17. T. Child, Optimising the management of patients with infertility. *The Practitioner* 2013, **257**. 19-22.

18. A. M. Propst, G. W. Bates, Evaluation and Treatment of Anovulatory and Unexplained Infertility. *Obstet. Gynecol. Clin. N. Am.* 2012, **39**. 507-519.

19. S. W. J. Van Rensburg, The role of delayed ovulation and anovulatory oestrus in the aetiology of functional infertility in bovines. *Papers. 3rd Internat. Congr. Anim. Reprod.* 1956. 52-53.

20. J. Singh, G. P. Adams, R. A. Pierson, Promise of new imaging technologies for assessing ovarian function. *Animal Reproduction Science* 2003, **78**. 371-399.

21. M. Malinouski, S. Kehr, L. Finney, S. Vogt, B. A. Carlson, J. Seravalli, R. Jin, D. E. Handy, T. J. Park, J. Loscalzo, D. L. Hatfield, V. N. Gladyshev, High-Resolution Imaging of Selenium in Kidneys: A Localized Selenium Pool Associated with Glutathione Peroxidase 3. *Antioxid. Redox Signal.* 2012, **16**. 185-192.

22. R. Evens, K. A. C. De Schamphelaere, B. De Samber, G. Silversmit, T. Schoonjans, B. Vekemans, L. Balcaen, F. Vanhaecke, I. Szaloki, K. Rickers, G. Falkenberg, L. Vincze, C. R. Janssen, Waterborne versus Dietary Zinc Accumulation and Toxicity in Daphnia magna: a Synchrotron Radiation Based X-ray Fluorescence Imaging Approach. *Environmental Science & Technology* 2012, **46**. 1178-1184.

23. D. Su, S. V. Novoselov, Q. A. Sun, M. E. Moustafa, Y. Zhou, R. Oko, D. L. Hatfield, V. N. Gladyshev, Mammalian selenoprotein thioredoxin-glutathione reductase - Roles in disulfide bond formation and sperm maturation. *Journal of Biological Chemistry* 2005, **280**. 26491-26498.

24. H. F. Irving-Rodgers, I. L. van Wezel, M. L. Mussard, J. E. Kinder, R. J. Rodgers, Atresia revisited: two basic patterns of atresia of bovine antral follicles. *Reproduction* 2001, **122**. 761-775.

25. L. J. Clark, H. F. Irving-Rodgers, A. M. Dharmarajan, R. J. Rodgers, Theca interna: The other side of bovine follicular atresia. *Biol. Reprod.* 2004, **71**. 1071-1078.

26. C. G. Ryan, Quantitative trace element imaging using PIXE and the nuclear microprobe. *International Journal of Imaging Systems and Technology* 2000, **11**. 219-230.

27. C. G. Ryan, Developments in dynamic analysis for quantitative PIXE true elemental imaging. *Nuclear Instruments and Methods in Physics Research Section B: Beam Interactions with Materials and Atoms* 2001, **181**. 170-179.

28. N. Hatzirodos, K. Hummitzsch, H. F. Irving-Rodgers, M. L. Harland, S. E. Morris, R. J. Rodgers, Transcriptome profiling of granulosa cells from bovine ovarian follicles during atresia. *BMC Genomics* 2014, **15**. 24

29. H. F. Irving-Rodgers, K. D. Catanzariti, M. Master, P. A. Grant, P. C. Owens, R. J. Rodgers, Insulin-like growth factor binding proteins in follicular fluid from morphologically distinct healthy and atretic bovine antral follicles. *Reprod. Fertil. Dev.* 2003, **15**. 241-248.

30. H. F. Irving-Rodgers, K. D. Catanzariti, W. J. Aspden, M. J. D'Occhio, R. J. Rodgers, Remodeling of extracellular matrix at ovulation of the bovine ovarian follicle. *Molecular Reproduction and Development* 2006, **73**. 1292-1302.

31. R. J. Rodgers, H. F. Irving-Rodgers, Morphological classification of bovine ovarian follicles. *Reproduction* 2010, **139**. 309-318.

32. K. M. Gebhardt, D. K. Feil, K. R. Dunning, M. Lane, D. L. Russell, Human cumulus cell gene expression as a biomarker of pregnancy

Metallomics Accepted Manuscript

outcome after single embryo transfer. *Fertility and sterility* 2011, **96**. 47-52 e2.

33. J. J. Ireland, R. L. Murphee, P. B. Coulson, Accuracy of predicting stages of bovine estrous cycle by gross appearance of the corpus luteum. *J. Dairy Sci.* 1980, **63**. 155-160.

34. S. Gromer, J. K. Eubel, B. L. Lee, J. Jacob, Human selenoproteins at a glance. *Cellular and Molecular Life Sciences* 2005, **62**. 2414-2437.

35. R. A. Sunde, A. M. Raines, K. M. Barnes, J. K. Evenson, Selenium status highly regulates selenoprotein mRNA levels for only a subset of the selenoproteins in the selenoproteome. *Bioscience Reports* 2009, **29**. 329-338.

36. G. Bermano, F. Nicol, J. A. Dyer, R. A. Sunde, G. J. Beckett, J. R. Arthur, J. E. Hesketh, Tissue specific regulation of selenoenzyme gene-expression during selenium deficiency in rats. *Biochemical Journal* 1995, **311**. 425-430.

37. R. K. Parshad, Effects of selenium toxicity on oestrous cyclicity, ovarian follicles, ovulation and foetal survival in rats. *Indian Journal of Experimental Biology* 1999, **37**. 615-617.

38. I. J. Rzepczynska, N. Foyouzi, P. C. Piotrowski, C. Celik-Ozenci, A. Cress, A. J. Duleba, Antioxidants Induce Apoptosis of Rat Ovarian Theca-Interstitial Cells. *Biol. Reprod.* 2011, **84**. 162-166.

39. S. Gupta, N. Malhotra, D. Sharma, A. Chandra, A. Ashok, Oxidative Stress and its Role in Female Infertility and Assisted Reproduction: Clinical Implications. *Int. J. Fertil. Steril.* 2009, **2**. 147-164.

40. A. Coskun, T. Arikan, M. Kilinc, D. C. Arikan, H. C. Ekerbicer, Plasma selenium levels in Turkish women with polycystic ovary syndrome. *Eur. J. Obstet. Gynecol. Reprod. Biol.* 2013, **168**. 183-186.

41. J. L. Tilly, K. I. Tilly, Inhibitors of oxidative stress mimic the ability of Follilce Stimulating Hormone to suppress apoptosis in cultured rat ovarian follicles. *Endocrinology* 1995, **136**. 242-252.

42. H. F. Irving-Rodgers, M. L. Harland, T. R. Sullivan, R. J. Rodgers, Studies of granulosa cell maturation in dominant and subordinate bovine follicles: novel extracellular matrix focimatrix is co-ordinately regulated with cholesterol side-chain cleavage CYP11A1. *Reproduction* 2009, **137.** 825-834.

43. C. M. Krest, E. L. Onderko, T. H. Yosca, J. C. Calixto, R. F. Karp, J. Livada, J. Rittle, M. T. Green, Reactive Intermediates in Cytochrome P450 Catalysis. *Journal of Biological Chemistry* 2013, **288**. 17074-17081.

44. K. E. Valdez, S. P. Cuneo, A. M. Turzillo, Regulation of apoptosis in the atresia of dominant bovine follicles of the first follicular wave following ovulation. *Reproduction* 2005, **130**. 71-81.

45. K. G. Hayashi, K. Ushizawa, M. Hosoe, T. Takahashi, Differential genome-wide gene expression profiling of bovine largest and second-largest follicles: identification of genes associated with growth of dominant follicles. *Reprod. Biol. Endocrinol.* 2010, **8**. 11.

46. G. V. Kryukov, S. Castellano, S. V. Novoselov, A. V. Lobanov, O. Zehtab, R. Guigo, V. N. Gladyshev, Characterization of mammalian selenoproteomes. *Science* 2003, **300**. 1439-1443.

47. Y. Gao, K. Walder, T. Sunderland, L. Kantham, H. C. Feng, M. Quick, N. Bishara, A. de Silva, G. Augert, J. Tenne-Brown, G. R. Collier, Elevation in tanis expression alters glucose metabolism and insulin sensitivity in H4IIE cells. *Diabetes* 2003, **52**. 929-934.

48. Y. H. Ye, Y. Shibata, C. Yun, D. Ron, T. A. Rapoport, A membrane protein complex mediates retro-translocation from the ER lumen into the cytosol. *Nature* 2004, **429**. 841-847.

49. Y. Gao, J. Pagnon, H. C. Feng, N. Konstantopolous, J. B. Jowett, K. Walder, G. R. Collier, Secretion of the glucose-regulated selenoprotein SEPS1 from hepatoma cells. *Biochem Biophys Res Commun* 2007, **356**. 636-641.

50. J. E. Curran, J. B. M. Jowett, K. S. Elliott, Y. Gao, K. Gluschenko, J. M. Wang, D. M. A. Azim, G. W. Cai, M. C. Mahaney, A. G. Comuzzie, T. D. Dyer, K. R. Walder, P. Zimmet, J. W. MacCluer, G. R. Collier, A. H. Kissebah, J. Blangero, Genetic variation in selenoprotein S influences inflammatory response. *Nature Genetics* 2005, **37**. 1234-1241.

51. J. Zeng, S. Du, J. Zhou, K. Huang, Role of SelS in lipopolysaccharide-induced inflammatory response in hepatoma HepG2 cells. *Arch Biochem Biophys* 2008, **478**. 1-6.

52. J. Liu, F. Li, S. Rozovsky, The Intrinsically Disordered Membrane Protein Selenoprotein S Is a Reductase in Vitro. *Biochemistry* 2013, **52**. 3051-3061.